Journal of Manufacturing Processes 49 (2020) 1–9

Contents lists available at ScienceDirect

Journal of Manufacturing Processes

journal homepage: www.elsevier.com/locate/manpro

Role of spot weld electrode geometry on liquid metal embrittlement crack development

C. DiGiovanni[a,*], L. He[a], U. Pistek[a], F. Goodwin[b], E. Biro[a], N.Y. Zhou[a]

[a] Department of Mechanical and Mechatronics Engineering, University of Waterloo, Waterloo, Canada
[b] International Zinc Association, Durham, NC, USA

ARTICLE INFO

Keywords:
Liquid metal embrittlement
Resistance spot welding
Advanced high strength steel

ABSTRACT

Advanced high strength steels (AHSS) used in automotive structural components are commonly protected using zinc coatings. However, the steel/zinc system creates the potential for liquid metal embrittlement (LME) during welding. Recent studies have examined the impact of the welding electrode geometry on LME cracking severity and found there to be some effect, but did not explore the responsible mechanisms for the changes. This work shows that a radius tip electrode provides minimal cracking while a truncated cone shape showed severe LME, particularly in the shoulder region. Thermo-mechanical simulations showed the significance of the thermal contact at the outer region of the electrode/sheet interface (weld shoulder). It was observed that when the water-cooled electrode presses into the steel during the welding, causing a contact between the steel surface and the electrode sidewall, a sudden local cooling of the weld shoulder occurs. This cooling causes contraction and tensile stresses on the material surface, leading to LME. Additionally, the magnitude and location of heat transfer between the steel and electrode is controlled by the thermal contact conductance.

1. Introduction

In recent years, environmental concerns about carbon emissions and fossil fuel usage led to regulations for lower vehicle fuel consumption [1,2]. One of the ways the industry is improving the fuel economy of their vehicles is by reducing vehicle weight, however mechanical performance of the materials and structures cannot be compromised. This has led to the development of advanced high strength steels (AHSS), which have higher strength than conventional steels. Their high strength allows AHSS parts to be made from thinner materials while maintaining part strength, so these steels have been increasingly implemented in automotive body-in-white structures [3,4]. In addition, AHSS are protected from the corrosive environment by a zinc coating. A thin layer of zinc provides cathodic protection to the underlying AHSS substrate.

The most common joining process associated with automotive assembly is resistance spot welding (RSW). In RSW, steel sheets are overlaid and clamped between two electrodes. A high current is then passed through the steel sheets to generate heat by Joule heating. The generated heat melts a volume of metal at the joint interface, forming a molten nugget. At the end of the weld cycle, the weld current is terminated and the joint remains clamped during the hold time, allowing the weld nugget to solidify under the force and cooling of the electrodes [5,6]. The addition of the zinc coating adds complexity to the welding process. During welding of AHSS, the zinc coating can lead to a cracking mechanism called liquid metal embrittlement (LME) [7,8]. Zinc melts at 419 °C, far below the melting point of the steel substrate (~1475 °C). During welding, the liquid zinc penetrates into AHSS grain boundaries, which are under tensile stresses from the RSW process; this allows LME cracks to open and propagate during RSW [9–11].

For LME to occur, three factors must be present: liquid zinc must be in direct contact with solid steel, the substrate must have a susceptible microstructure, and the substrate must be under tensile stresses [12,13]. Tensile stresses have particularly been observed to accentuate LME cracking [14]. The welding process causes two of these factors (liquid zinc and tensile stresses) to occur. Therefore, the welding parameters have a large influence on LME crack formation during RSW. Barthelmie et al. (2016) [15] showed that using a larger electrode face diameter reduced cracks by 50 %. Similar results were observed by Sierlinger *et. al* (2016) [16] who used an increased electrode face diameter to reduce LME cracking. Likewise, Kim et al. (2014) [12] observed decreased LME severity with increasing electrode diameter. However, it is unclear if all welds in this test were made using the same heat input (and by association nugget size), which needs to be controlled for a direct assessment [13]. If heat input was not held constant during these studies, the observed reduced LME cracking may be due to

* Corresponding author.
E-mail address: ctdigiov@uwaterloo.ca (C. DiGiovanni).

https://doi.org/10.1016/j.jmapro.2019.11.015
Received 26 August 2019; Received in revised form 28 October 2019; Accepted 16 November 2019

decreased heat input, as the researchers used a larger electrode diameter which decreases current density. Murugan et al. (2018) [17] found that cracking decreased with increasing electrode radius. Additionally, it was shown that cracking was further reduced when electrode curvature was increased due to a reduction in current density at the edge of the electrode contact area. Temperature and stress were decreased at that location.

Previous work by Barthelmie et al. (2016) [15], Kim et al. (2014) [12] and Murugan et al. (2018) [17] showed a relationship between electrode geometry and LME cracking severity, however, LME severity in welds made with various electrode types needs to be explored under constant heat input conditions. In the present study, welds made using three standard electrode types (B-nose, truncated cone, and radius) were compared for LME severity, as calculated from observations of LME crack length and frequency at the various locations around the weld. The mechanism for the observed cracking was explained using thermo-mechanical modelling, using the commercial RSW simulation software Sysweld®. The observations from both the experimental and simulation work were combined to provide key insights into the stress development during resistance spot welding and the process conditions for the onset of LME cracking.

2. Materials and methods

2.1. Materials

This study was carried out on GI coated TRIP1100 AHSS, as it is highly susceptible to LME shown in previous work [18,19] and is of interest to industry. The chemical composition and mechanical properties can be found in Table 1 below.

2.2. Electrode geometries and weld schedule

Three distinct electrode types were selected for the study: B-nose, truncated cone and radius tip electrodes. A schematic drawing of each electrode is shown in Fig. 1. To ease the process of keeping heat input constant, the same electrode face diameter of 7 mm was selected for both the B-nose and truncated cone type. Keeping heat input constant allows for an isolated comparison of how each electrode type affects LME cracking. The weld schedule for the standard case is shown in Table 2, and the current was adjusted for the radius electrode to match the heat input.

Welding was carried out using a 250 kVA, 60 Hz single phase AC pedestal resistance spot welder. The TRIP1100 was sheared into 25 × 25 mm coupons for welding. The welding schedule was developed based on the A/SP AC starting weld schedules [20] at a heat input just below the expulsion current (I_{max} -250A) for the B-nose electrode. This heat input was selected to promote LME cracking for clear observation while not exceeding the maximum expulsion current (I_{max}). For a fair comparison between the electrode types, the current was adjusted for the cone and radius electrode (if needed) so the nugget size was the same for all cases. A weld nugget size of 7.4 ± 0.1 mm was produced for all samples.

Samples were cross-sectioned along the plane which includes the most LME cracks and prepared using standard metallography techniques to observe and measure LME cracking in the weld area. LME severity was quantified from crack measurements from nine welds made using identical parameters using the LME crack index [21]. Measurements were taken for both the crack depth and number of cracks, which have both proven to be an important factor in LME severity [22–24]. The crack index holistically quantifies LME cracking of a welded cross-section so an accurate comparison can be made between welding conditions. The crack index is defined as:

$$CI = \frac{nL}{\tau} \quad (1)$$

Where n is the mean number of cracks per sample, L is the lognormal median crack depth and τ is the sheet thickness.

2.3. Welding process simulations

To study the cracking phenomena during spot welding, the RSW process was simulated using an axisymmetric finite element method (FEM) model. The critical conditions for the characterization of LME at the electrode-sheet interface was defined as the simultaneous presence of surface temperatures exceeding 419 °C (melting temperature of zinc) and tensile stresses; this is a similar methodology used in previous work [13,25,26]. The temperature and stress distributions experienced during RSW were simulated using the commercial finite element software package Sysweld®, designed to simulate the RSW process. A mesh was generated using the software's RSW tool which included 2306 2D quad-tria linear elements for the B-Nose case, 2280 elements for the truncated cone, and 2572 elements for the radius electrode. Temperature dependent material properties for recently developed AHSS (such as TRIP1100) are not widely available and determining them experimentally can be cumbersome and time-consuming. For this study, the material properties were calculated using the material properties simulation software JMatPro®. The results of the key temperature dependent properties for TRIP1100 are shown in Fig. 2, which shows reasonable values and typical trends for AHSS. The simulation predicted a nugget size of 7.45 mm which is within the range of the experimental results. To further validate the model, the cross-sections of the experimental and simulated results are compared in Fig. 3, showing a similar shape in nugget and heat affected zone.

3. Results and discussions

3.1. Liquid metal embrittlement severity

Significant differences in LME cracking were observed for each electrode type. The results showed a clear impact of electrode geometry on the overall LME severity, where welds made using the radius electrode show the least LME cracking. The results are summarized in Fig. 4. The lower LME severity of the welds made using the radius electrode is consistent with previous work [17], but it is important to note the distinction between the cracking observed in welds made with B-nose and truncated cone electrode. The geometry of the electrode shoulder is the only distinction between the B-nose and cone electrode; the electrode face is identical between the two. Similar results would therefore be expected for cracking in the center region however cracking observed in the shoulder region of the respective welds was observed to be quite different. To further investigate the differences in

Table 1
Material examined.

Material	Main alloying elements (wt.%)					
TRIP1100	C	Mn	Si	Cr	Al	Mo
	0.20	2.17	1.61	0.03	–	–
	Mechanical Properties					
	Thickness (mm)	Yield Strength (MPa)	Tensile Strength (MPa)	% Elongation	Top coating thickness (g/m^2)	Bottom coating thickness (g/m^2)
	1.6	861	1100	14.6	58	70

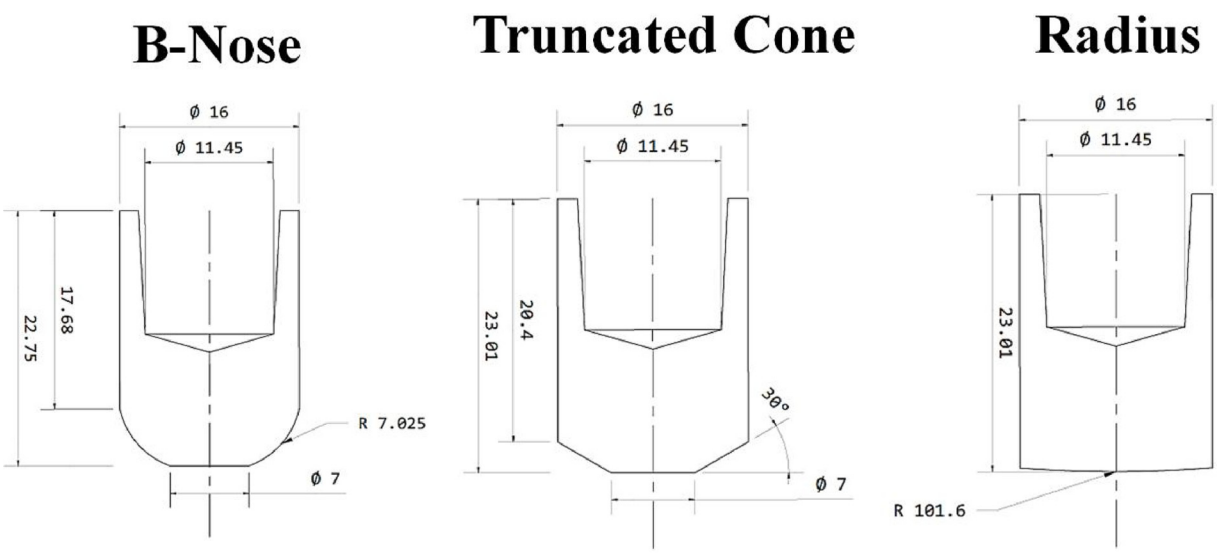

Fig. 1. Schematic of each electrode investigated (all dimension in mm).

Table 2
Welding schedules used for the study.

Material	Current (kA)	Time (cyc)	Force (kN)	Hold Time (cyc)
TRIP1100	11.5	7-1-7-1-7	4.2	10

LME crack distribution, the crack index was calculated for the center and shoulder region for each electrode type. The results showed clear differences in the locations of severity, which is directly related with electrode shoulder geometry. Experimental cross-sections of the weld samples and the localized LME crack index results are plotted in Fig. 5.

The weld cross-section images and crack index plots in Fig. 5 show that changing electrode types caused different LME cracking patterns.

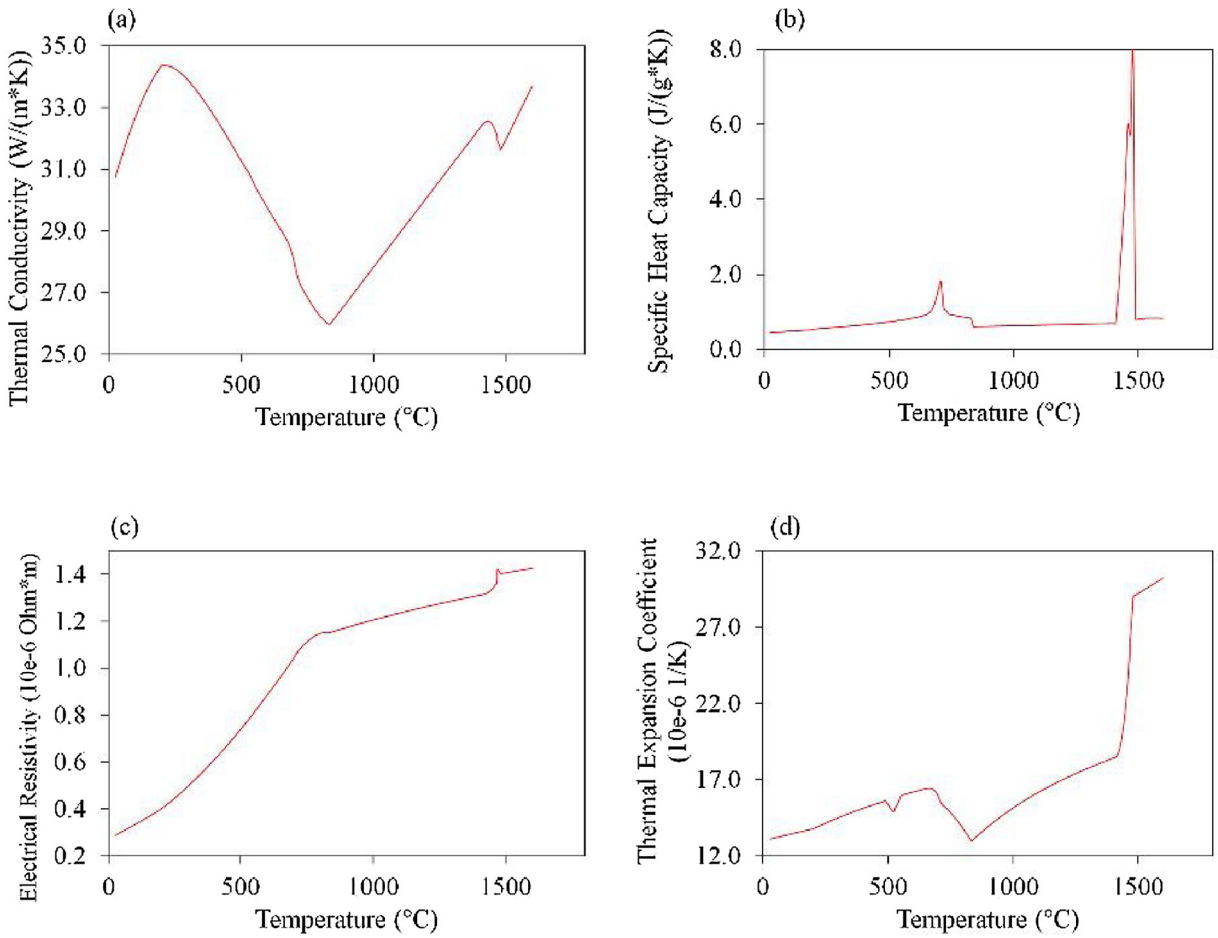

Fig. 2. Key material properties for RSW (a) Thermal conductivity (b) Specific heat capacity (c) Electrical resistance (d) Thermal expansion coefficient.

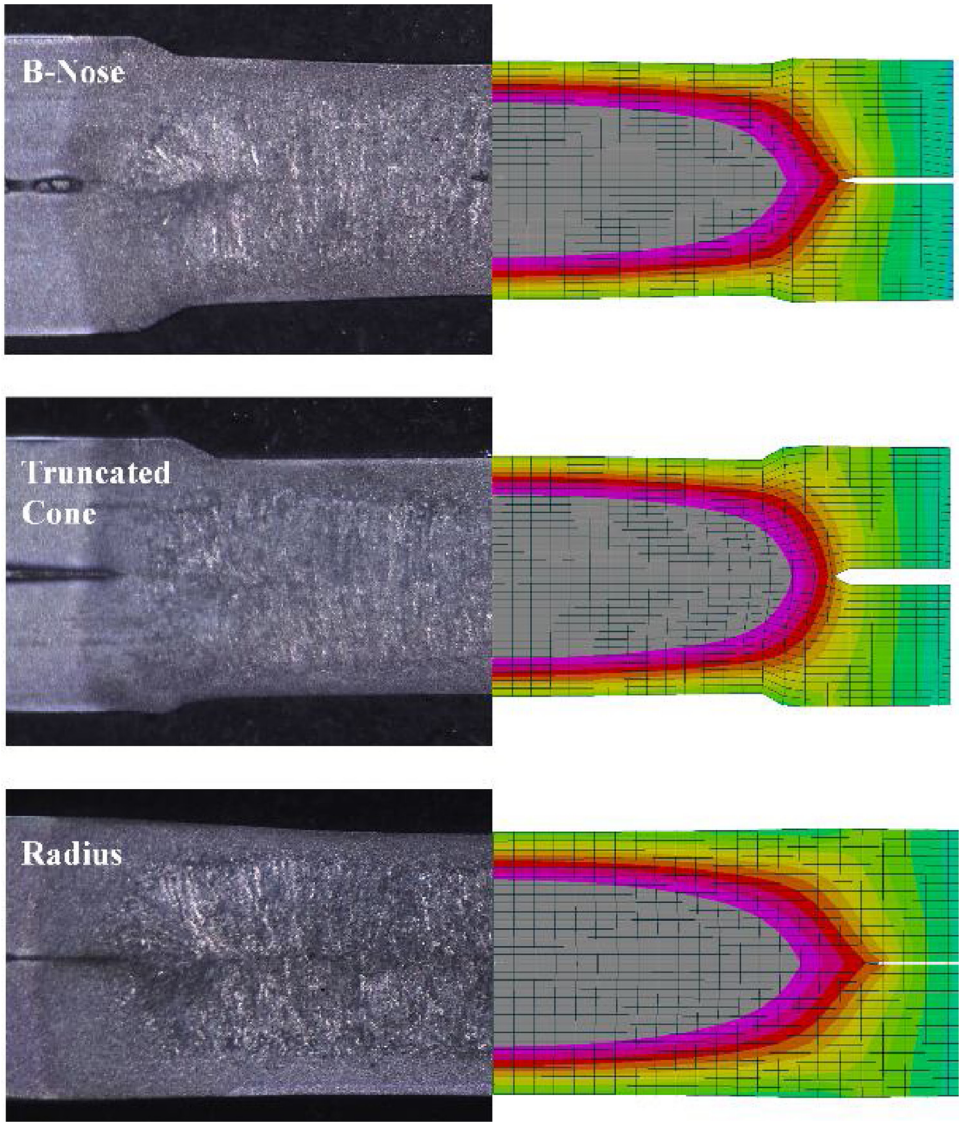

Fig. 3. Validation of cross-sections between experimental results and simulation results for each electrode type.

Clearly, no shoulder cracking occurs in the radius electrode case, and minimal cracking was observed in the center region. The radius electrode provides the best option for LME reduction. As expected, similar cracking severity levels were seen in the centre region of both the B-nose and truncated cone. However, when comparing the cracking severity from the weld shoulder, there is a clear increase in severity in welds made using the cone type electrode as compared to the B-nose. Since the only difference between the two cases is the weld shoulder geometry, it can be stated that a truncated cone shaped shoulder leads to worse LME cracking compared to the B-nose. When comparing shoulder cracking in the experimental cross-sections in Fig. 5(a) and (b), it was observed that the shoulder cracking in (b) is further outside the indent compared to (a). Additionally, cracks are commonly observed on the outer portion of the electrode indent in previous work

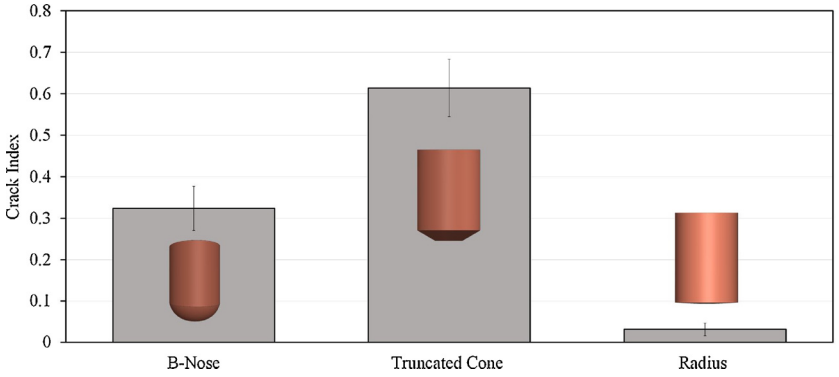

Fig. 4. LME severity for each electrode case.

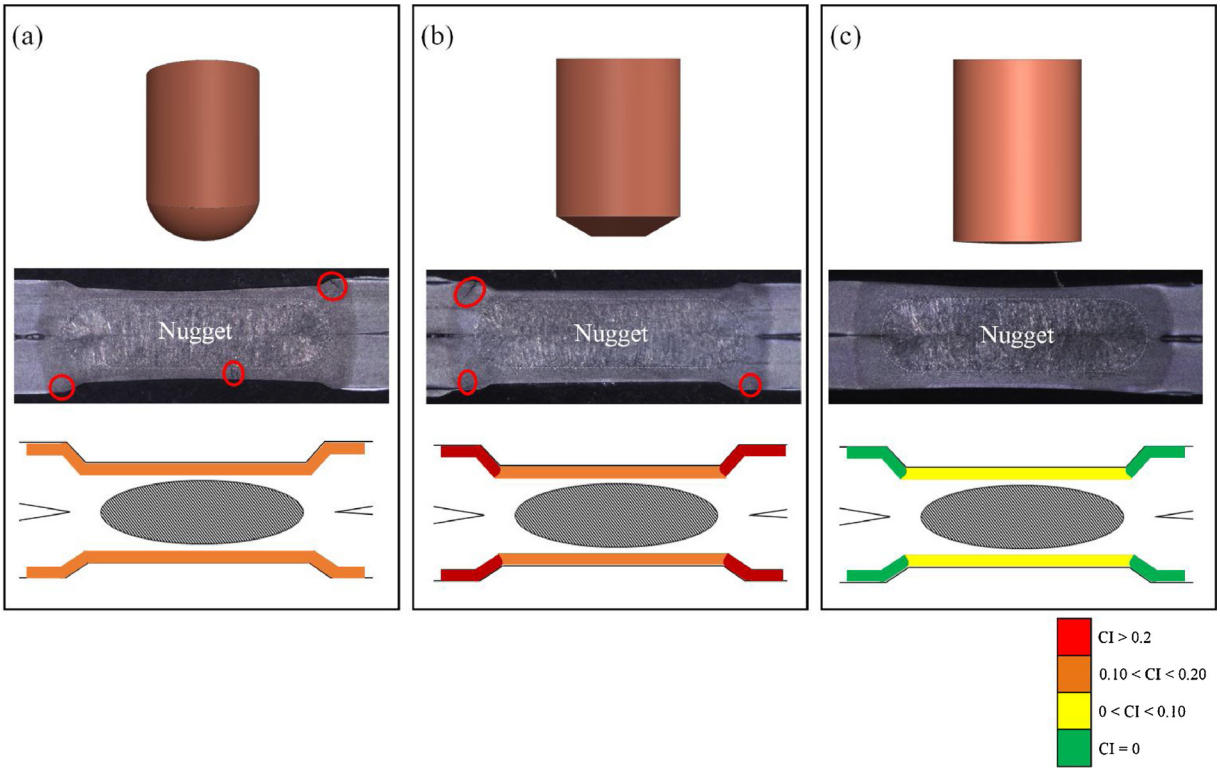

Fig. 5. Weld cross-section and localized LME crack index for (a) B-nose electrode type (b) truncated cone (c) radius tip electrode.

using cone shaped electrodes [27,28] but it has not been reported for B-nose electrodes. Further RSW process analysis is needed to gain insight into this observation.

Overall, the experimental evidence shows that electrode geometry governs LME severity. However, the link between electrode geometry and LME severity is unclear. It is well established in literature that temperature and stress are the governing process factors for the onset of LME during welding [13,29]. Therefore, a more detailed thermo-mechanical analysis of the welding process is needed to understand how changing electrode geometries impacts LME crack development.

3.2. Welding process simulations

To further investigate the thermo-mechanical differences at the steel surface during the welding cycle made with different electrode types, the welding process was simulated using the Sysweld® software. A temperature and stress plot result for the shoulder area of interest is shown in Fig. 6. This plot shows that the various electrodes result in different temperature and stress responses in the steel during the welding process. The stress results presented are perpendicular to the thickness direction of the sheet, since that is the stress component responsible for LME cracking.

When comparing the electrodes, it may be seen that the temperature and stress plots at the shoulder of welds made with the radius electrode are fundamentally different than those from welds made with the B-nose and truncated cone electrodes. The shoulders of the welds made with radius electrodes experienced temperatures that stayed close to or below the melting of zinc (419 °C) and stresses were compressive, except for a brief period during initial stage of welding. These characteristics are due to the unique contact of the radius shaped electrode. In contrast, both the B-nose and truncated cone electrode show consistent heating (apart from the cooling between the pulses) until a sudden drop in temperature is observed towards the end of the weld time. This sudden drop in temperature is accompanied by a sudden increase in tensile stress. The large temperature drop is due to

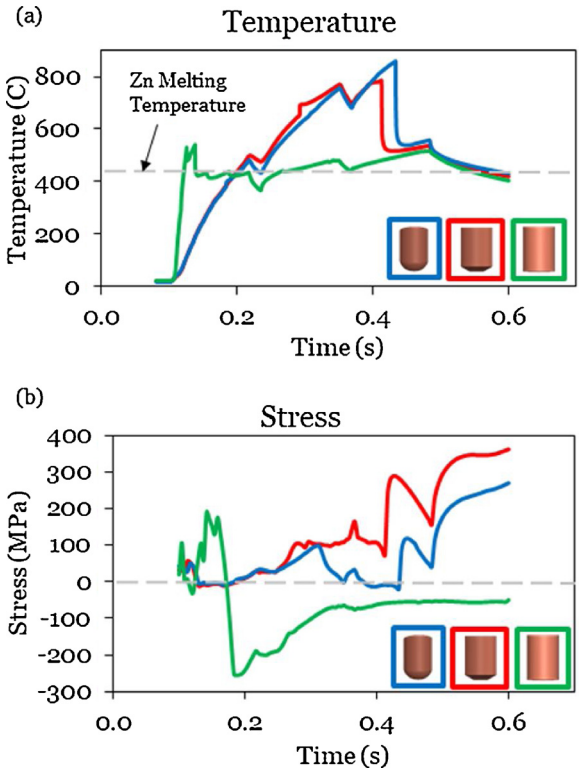

Fig. 6. Plots for (a) temperature in the weld shoulder area (b) stress perpendicular to the thickness direction.

mechanical collapse from material softening in the sheet steel, causing the electrode to press further into the steel, which creates a new thermal contact at the shoulder. This is shown graphically for the cone electrode in Fig. 7. After this point, all three temperature curves

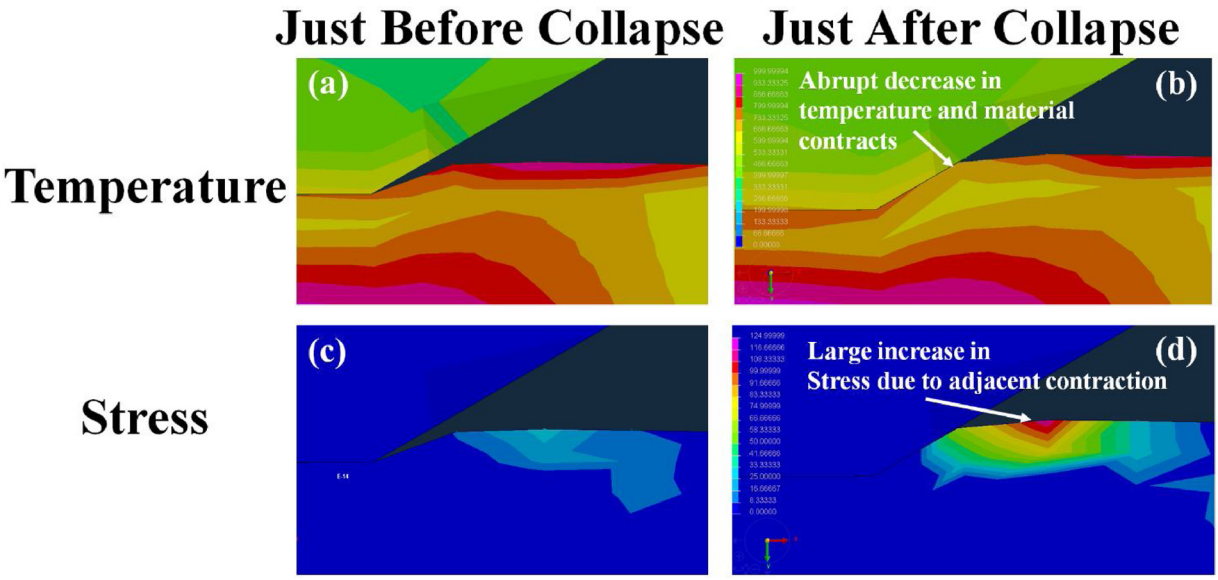

Fig. 7. Temperature and stress (a) Temperature plot at the location of shoulder cracks just before collapse (b) temperature field at the instant just after collapse (c) stress field just before collapse (d) stress field just after the collapse showing increase in stress.

converge as shown in Fig. 6, since they all have direct contact with the electrode, which is extracting heat from the weld.

Electrode collapse not only affected shoulder temperature, but it also increased the tensile stresses. Fig. 7 shows that increased cooling resulted in a peak stress in the steel away from the electrode/sheet contact, where fastest cooling rate occurred. This phenomenon of sudden cooling with the resulting stress can best be explained in its basic form with a schematic of the material movement during the welding process. In Fig. 8 shows a string of elements represented the material at the top surface of the sheet during welding before collapse. At this time the whole region is hot and is at equilibrium. Once electrode collapse occurs, the element on the left suddenly cools and contracts. The contraction of the left element results in the neighboring hot elements being stretched into tension to accommodate the volume change of the cooler elements. This causes the greatest increase in tensile stress in the element which did not experience any contraction as it needs to have the greatest compensation for the cold elements' contraction. Far from the peak stressed element, the elements no longer carry the tensile load and there is no increase in tensile stress due to the contraction of the cold element. From this analysis, it may be seen that the stresses are primarily thermally driven as opposed to mechanically driven, as they are caused by the new thermal contact between the electrode and sheet, leading to a sudden cooling in the weld shoulder.

The temperature and stress field results show the key role of electrode geometry in LME severity and provides insight on the experimental results. The shape of the electrode shoulder controls the formation of LME cracks as it governs contact conditions between the electrode and sheet at the shoulder. Previous work on electrode force by Choi et al. (2018) [26] has also shown the thermal aspects of the RSW process to be dominant as more severe LME was observed when welding using low electrode force. Although the mechanical force of the electrode was decreased, the temperature and thermal stress in the steel were much higher. It is therefore not surprising that a thermally dominant mechanism drives LME when the influence of electrode geometry is studied. The radius type electrode proved to be the best for reducing LME cracking because of its consistent contact throughout the welding process. The electrode contacts the sheet early in the process and cools the sheet continuously throughout the welding cycle. However, the differences between the weld shoulder contact of the B-nose and cone type electrode should be investigated in more detail.

3.3. Influence on crack location

When comparing the stress field plots of the truncated cone and B-nose electrodes, a subtle yet significant difference is observed. A stress field comparison between the electrode types showed a shift in the location of highest stress, as shown in Fig. 9. In the case of the truncated cone electrode, the location of highest stress is further out from the weld shoulder compared to the B-nose case. A similar pattern was observed for the location of LME cracks in the experimental work (mentioned in Section 3.1 and shown in Fig. 5), however there was no clear experimental explanation for the change in location. The shift in the location of highest stress shown from the process simulation explains the differences in shoulder crack location.

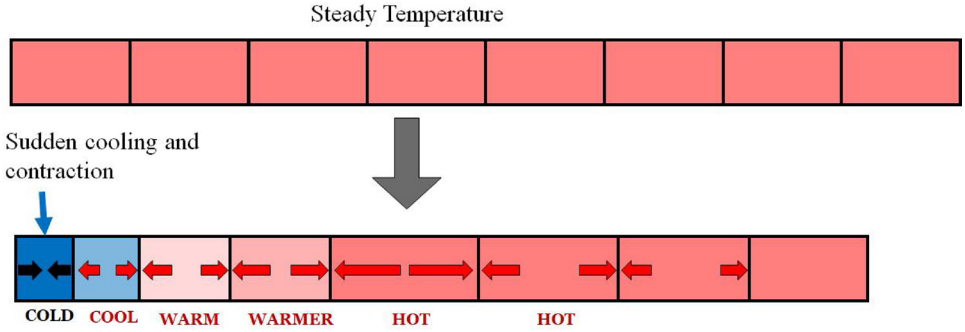

Fig. 8. Basic illustration of thermal contraction and tensile stresses in neighboring elements.

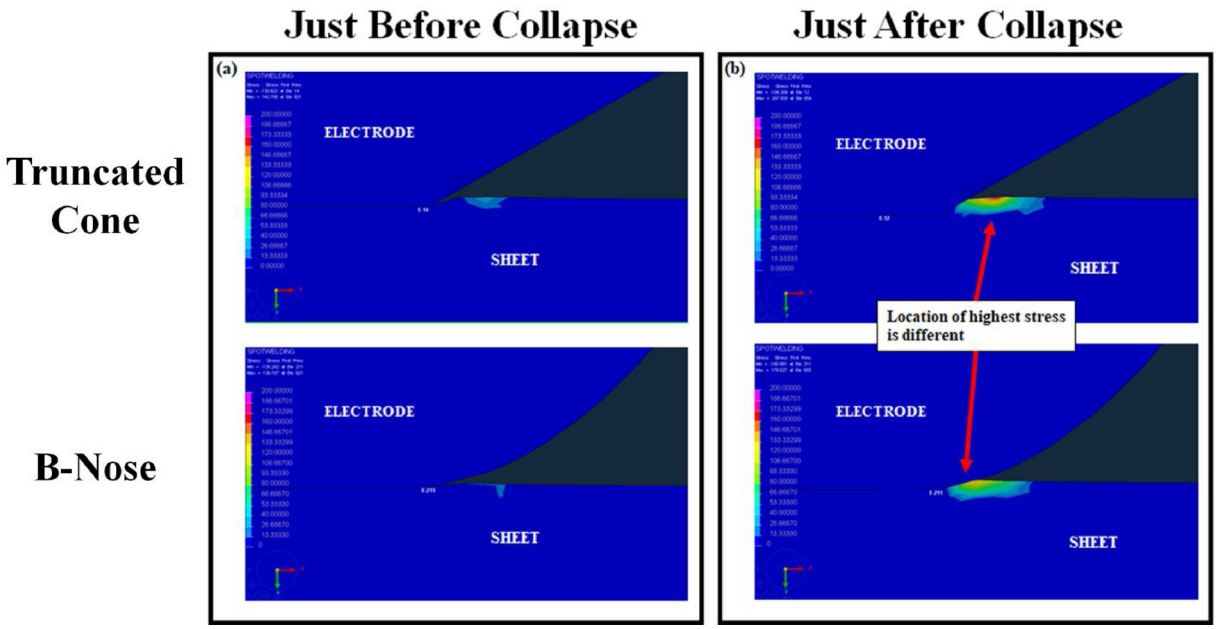

Fig. 9. Comparison of stress fields for cone and B-nose electrode (a) before collapse (b) instant after collapse showing different peak stress locations.

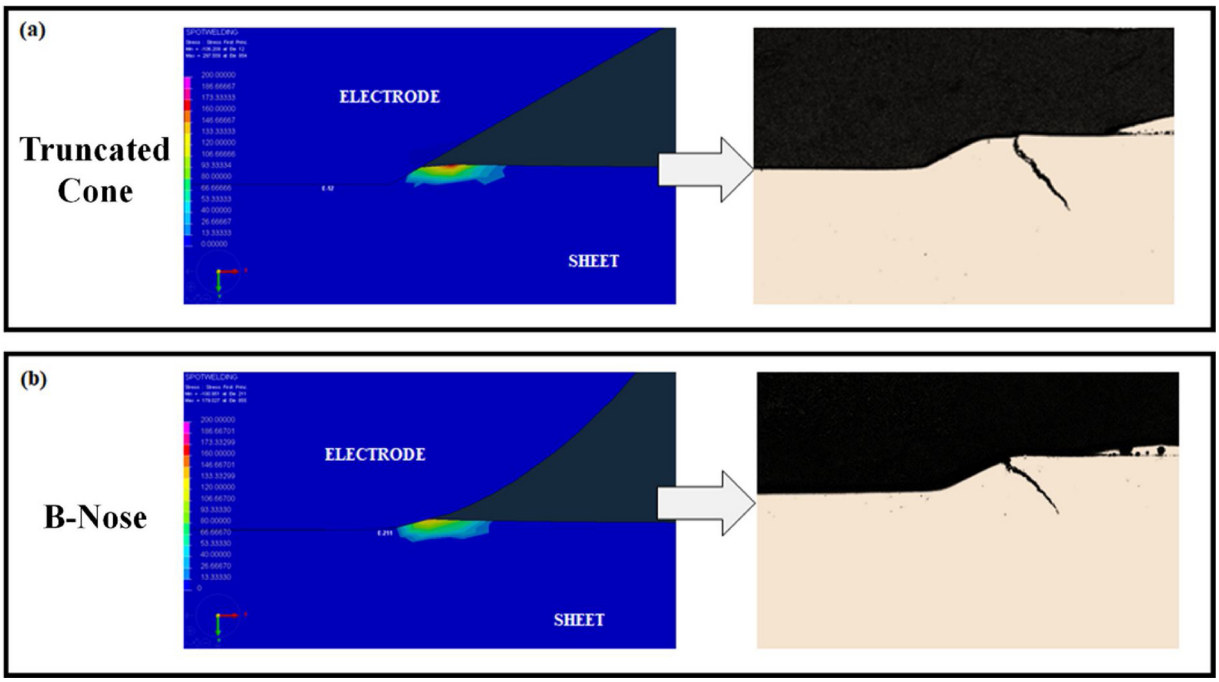

Fig. 10. Comparison of the stress field simulation and experimental results for LME cracking (a) cone type electrode (b) B-nose electrode.

Both the truncated cone and B-nose electrode experience the same thermo-mechanical phenomenon leading to tensile stresses in the shoulder region. However, the shift in stress location leads to a shift in LME cracking location as shown in Fig. 10. The location of peak stress from the process simulation directly matches the experimental LME cracking location, but it is unclear why the shift in stress location occurred. To gain further insight, the factors that govern thermal contact during the process simulation need to be examined.

In order for a shift in location of stress to occur the location of heat transfer to the electrode must be different. As all other process variables are the same, the effects of electrode geometry on thermal contact are examined. The efficiency of thermal contact conductance is highly dependent on the contact pressure between two bodies [30]. To further investigate the thermal contact conductance, the plots of pressure and heat flux were examined which are shown in Fig. 11. For the truncated cone, there is a pressure concentration at the corner of the electrode face and electrode shoulder. Additionally, high pressure from the electrode continues up the weld shoulder of the sheet. The high pressure leads to efficient cooling along the entire length of the weld shoulder area, resulting in the entire weld shoulder contracting due to negative thermal expansion. Since the weld shoulder is the area contracting, the tensile stresses occur away from the weld shoulder as described in Section 3.2. Conversely, the B-nose electrode has low pressure along the length of the weld shoulder which leads to the cooling and contracting under the electrode face and at the lower edge of the weld shoulder. This leads to tensile stresses at the top of the weld shoulder. Due to the difference in pressure profile from each electrode, the location of material cooling and contraction shifts, resulting in a

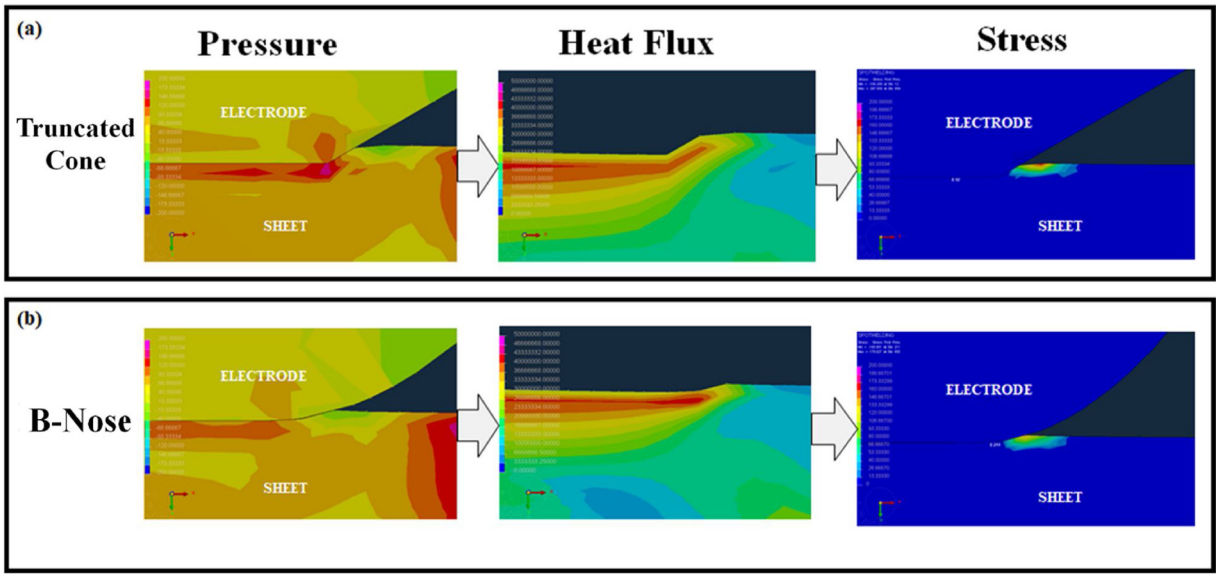

Fig. 11. Pressure, heat flux and stress fields the instant after collapse for the (a) cone electrode (b) B-nose electrode.

shift of high stresses.

The investigation into electrode geometry not only showed new insights in LME shoulder cracking but also into the mechanism that governs crack location in the shoulder. Discrepancies between different locations of shoulder cracks can now be explained with regards to the RSW process. Furthermore, the insights gained on the heat transfer and mechanics of the electrode/sheet interface can be used for further work on LME reduction. Since the mechanism of crack formation is better understood, researchers can work to apply these insights into reduction methods.

4. Conclusion

From the experimental results, electrode geometry governs the overall LME severity and the crack location distribution. A considerable reduction in LME cracking was observed for the radius electrode, while welds made with the B-nose and truncated cone type electrode experienced similar LME cracking in the center region and welds made with the truncated cone showed severe LME cracking in the shoulder area. Simulations of the stress and temperature field showed that the consistent contact of the radius electrode led to lower temperatures and compressive stresses in the shoulder area during welding, which led to a reduction in LME cracking. Additionally, the simulations showed stresses in the shoulder area of welds made with the B-nose and truncated cone cases are due to the sudden cooling of the sheet as the electrode presses into it. This led to material contraction and tensile stresses adjacent to the welds shoulder. Finally, it was determined that the location of high stress in the shoulder is also dependent on electrode geometry, as cracks in the welds made with the cone were found on the outer region of the electrode indent and in the B-nose case were located at the indent. This found to be due to a difference in contact conditions between the steel sheet and the electrode at the weld shoulder.

Declaration of Competing Interest

The authors declare that they have no known competing financial interests or personal relationships that could have appeared to influence the work reported in this paper.

Acknowledgements

The authors would like to acknowledge the International Zinc Association (IZA) for their financial support and donation of material of this study, ESI for access to the thermo-mechanical RSW process simulation software Sysweld®, the Natural Sciences and Engineering Research Council of Canada (NSERC) and Canada Research Chairs (CRC) program for their support.

References

[1] Cooper AI. Materials chemistry: cooperative carbon capture. Nature 2015;519:295.
[2] Creutzig BF, Jochem P, Edelenbosch OY, et al. Transport: a roadblock to climate change mitigation? Science (80-.) 2015;350:911–2.
[3] Parkes D, Westerbaan D, Nayak SS, et al. Tensile properties of fiber laser welded joints of high strength low alloy and dual-phase steels at warm and low temperatures. Mater Des 2014;56:193–9.
[4] Parkes D, Xu W, Westerbaan D, et al. Microstructure and fatigue properties of fiber laser welded dissimilar joints between high strength low alloy and dual-phase steels. Mater Des 2013;51:665–75.
[5] Kimchi M, Phillips DH. Resistance spot welding, fundamentals and applications for the automotive industry. Columbus, Ohio, USA: Morgan Claypool Publ.; 2017.
[6] Zhang H, Senkara J. Resistance welding: fundamentals and applications. 2012.
[7] Kim YG, Kim IJ, Kim JS, et al. Evaluation of surface crack in resistance spot welds of Zn-coated steel. Mater Trans 2014;55:171–5.
[8] Jiang C, Thompson aK, Shi MF, et al. Liquid metal embrittlement in resistance spot welds of AHSS steels. AWS Prof Progr 2003. p. 9A.
[9] Ina K, Koizumi H. Penetration of liquid metals into solid metals and liquid metal embrittlement. Mater Sci Eng A 2004;387–389:390–4.
[10] Joseph B, Barbier F, Dagoury G, et al. Rapid penetration of liquid Bi along Cu grain boundaries. Scr Mater 1998;39:775–81.
[11] Beal C, Kleber X, Fabregue D, et al. Embrittlement of a zinc coated high manganese TWIP steel. Mater Sci Eng A 2012;543:76–83.
[12] Kim YG, Kim IJ, Kim JS, et al. Evaluation of surface crack in resistance spot welds of Zn-coated steel. Japan Inst Met Mater 2014;55:171–5.
[13] Ashiri R, Haque MA, Ji C-W, et al. Supercritical area and critical nugget diameter for liquid metal embrittlement of Zn-coated twining induced plasticity steels. Scr Mater 2015;109:6–10.
[14] Frei J, Biegler M, Rethmeier M, et al. Investigation of liquid metal embrittlement of dual phase steel joints by electro-thermomechanical spot-welding simulation electro-thermomechanical spot-welding simulation. Sci Technol Weld Join [Internet] 2019;24:624–33. https://doi.org/10.1080/13621718.2019.1582203. Available from:.
[15] Barthelmie J, Schram A, Wesling V. Liquid metal embrittlement in resistance spot welding and hot tensile tests of surface-refined TWIP steels. IOP Conf. Ser. Mater. Sci. Eng. [Internet] 2016:118. Available from: http://stacks.iop.org/1757-899X/118/i=1/a=012002?key=crossref.1f5242fc96a01ffcaf40f823cecc5822.
[16] Sierlinger R, Gruber M. A cracking good story of liquid metal embrittlement during spot welding of advanced high strength steels. Tech Rep Stahl GmbH 2016.
[17] Murugan S, Mahmud K, Park Y-D. The influence of electrode geometry on liquid metal embrittlement cracking in resistance spot welding of advanced high strength steel. Int Inst Weld Annu Meet. 2018. p. III-1876-18.
[18] DiGiovanni C, Biro E, Zhou N. Impact of liquid metal embrittlement cracks on resistance spot weld static strength. Sci Technol Weld Join 2018.
[19] Wintjes E, DiGiovanni C, He L, et al. Quantifying the link between crack distribution and resistance spot weld strength reduction in liquid metal embrittlement

susceptible steels. Weld Word 2019.
[20] A/SP starting resistance spot weld schedules for AHSS. Auto/Steel Partnership; 2014. p. 1.
[21] Wintjes E, DiGiovanni C, He L, et al. Quantifying the link between crack distribution and resistance spot weld strength reduction in liquid metal embrittlement susceptible steels. Weld World 2019;63:807–14.
[22] Choi D-Y, Uhm S-H, Enloe CM, et al. Liquid metal embrittlement of resistance spot welded 1180TRIP steel- effects of crack geometry on weld mechanical performance. Mater Sci Technol 2017:454–62.
[23] DiGiovanni C, Han X, Powell A, et al. Experimental and numerical analysis of liquid metal embrittlement crack location. J Mater Eng Perform [Internet] 2019. https://doi.org/10.1007/s11665-019-04005-2 Available from:.
[24] DiGiovanni C, Biro E, Zhou NY. Impact of liquid metal embrittlement cracks on resistance spot weld static strength strength. Sci Technol Weld Join [Internet] 2019;24:218–24. https://doi.org/10.1080/13621718.2018.1518363. Available from:.
[25] Choi D, Sharma A, Jung JP. Parametric study for liquid metal embrittlement. Sheet Met. Weld. Conf. XVIII. Livonia. 2018. p. 1–9.
[26] Choi DY, Sharma A, Uhm SH, et al. Liquid metal embrittlement of resistance spot welded 1180 TRIP steel: effect of electrode force on cracking behavior. Met Mater Int 2018.
[27] Benlatreche Y, Duchet M, Dupuy T, et al. Effect of liquid metal embrittlement cracks on the mechanical performances of spot welds. 5th Int. Conf. Steels Cars Truck. 2017.
[28] Benlatreche Y, Ghassemi-Armaki H, Duchet M, et al. Spot-weld integrity of Zn-coated 3rd Gen. Advanced high strength steel in presence of LME. Int Automot Body Congr (IABC 2017 Dearborn) 2017:9–18.
[29] Beal C. Mechanical behaviour of a new automotive high manganese TWIP steel in the presence of liquid zinc. 2011.
[30] Wang A, Zhao J. Review of prediction for thermal contact resistnace. Sci China Ser A-mathematics Phys Astron Technol Sci 2010;53:1798–808.